JOURNAL OF MATERIALS SCIENCE 24 (1989) 1207–1218

Intrinsic toughness of interfaces between SiC coatings and substrates of Si or C fibre

A. S. ARGON, V. GUPTA, H. S. LANDIS*, J. A. CORNIE
Department of Mechanical Engineering, Massachusetts Institute of Technology, Cambridge, Massachusetts 02139, USA

The critical energy release rate for separation of SiC coatings from single crystal Si substrates or surfaces of carbon fibres, along their well-defined interfaces can be determined quite accurately from analysis of the spontaneous delamination of coatings under bi-axial stress, when such coatings exceed a critical thickness. Direct evaluations have been made of the specific work of delamination along the interface for SiC coatings from single crystal Si substrates, for both the case of coatings under bi-axial compression, as well as under bi-axial tension. The critical energy release rate for coatings in tension was 5.1 J m^2, and that for coatings under compression was 5.9 J m^2. The higher value of the latter is attributed to relative slippage between coating and substrate before lift-off of the former. Corresponding determination of the critical energy release rate for delamination of SiC coatings under bi-axial tension from surfaces of anisotropic Pitch-55 carbon fibres gave an answer of 5.5 J m^2. These values compare very well with expectations from surface energies of strong solids.

1. Introduction

Relaxation of shear tractions across interfaces and eventual fracture along interfaces are key phenomena affecting the performance of composites reinforced with stiff or less deformable heterogeneities. Particularly, the possibility of controlled delamination along an interface of a reinforcing fibre or platelet before the stresses become too high in them to produce fracture has been recognized for some time as a desirable condition to achieve stable traction-displacement behaviour, and to increase overall toughness. In the composites field, key interface properties are usually measured by simple operational procedures, such as a single fibre pull-out test or a relatively macroscopic interlaminar shear test [1]. There have also been other more indirect techniques, such as the periodic cracking of a brittle fibre embedded in a matrix, plastically extended parallel to the fibre [2], or initiating local interface fractures through very local deformations produced by scratches [3] or hardness indenters [4]. In all of these cases, either only average information is obtained for a delamination process in which, in reality, a front of concentrated stresses and inelastic strain progagate along the interface, or the deformation is even more inhomogeneous and produces local interface separation through the production of a plastic misfit, which requires the solution of local elasto-plastic boundary value problems for the evaluation of the critical interface conditions. In all of these instances, the critical interface tractions that result in separation are not accurately determinable, whilst the fracture toughness of the interface itself is usually shrouded by much excess accompanying deformation, often even absent in the failure process occurring in the prototype composite.

In many interface fractures resulting in a clean cleavage-like separation, the critical intrinsic energy release rate G_{co} for separation of the interface (to be referred to here as the *intrinsic interface toughness*), is accompanied by a much larger term, G_p, reflecting the dissipative additional inelastic deformations in the layers immediately adjacent to the separating interface. Whilst this additional work, G_p, can dominate over the toughness G_{co}, the latter still scales the much larger inelastic dissipation work, so that any factor which affects G_{co} is directly reflected in the magnitude of G_p in an amplified manner [5, 6]. In an accompanying communication [6], we have proposed that the toughness of interfaces between protective coatings, such as SiC and fibres such as Pitch-55, can be tailored to initiate controlled delamination to protect the fibre from damage, and thereby act as mechanical fuses. There, we discussed an experimental technique based on the double cantilever beam to measure the overall specific fracture work ($G_{co} + G_p$) of model composite interfaces. Here, we will discuss special techniques on how the much smaller, but key, intrinsic toughnesses G_{co} of interfaces can be measured, which must be governed to control composite properties.

2. Intrinsic mechanical properties of interfaces

2.1. Toughness of coating – substrate interfaces

During the study of vapour deposition of SiC coatings on various substrates, it became clear that the intrinsic toughness of an interface between a thin coating and

* *Present address*: General Telephone and Electronics Laboratory, Waltham, Massachusetts, USA.

a more massive substrate is directly measurable through the controlled delamination of the coating from the substrate during the relief of the residual stresses in the coating. Such delaminations and their potential for interface toughness measurement were recognized earlier by Evans and Hutchinson [7] for surface layers under residual compression. Here, we will demonstrate how this technique can be generalized and used for intrinsic interface toughness measurement in cases where the coating is either in residual tension or residual compression, on both model systems as well as on actual prototype interfaces between SiC coatings and Pitch-55 fibres. Before we present the details of such interface toughness determinations, it is necessary to discuss some essential details of the coating process which clarifies the origin of the residual stresses.

2.2. Vapour deposition of SiC coatings

Amorphous hydrogenated thin films of SiC were deposited on Pitch-55 fibres and on Si single crystal wafers using a plasma-assisted chemical vapour deposition (PACVD) process, the details of which are discussed [8]. It was observed that the processing parameters, especially the ion bombardment energy play a critical role in determining the unique physical and mechanical properties of the SiC deposits. These processing parameters could be adjusted to obtain the necessary toughness properties for the interfaces to optimize their desirable mechanical fuse action discussed in the accompanying communication [6].

Preliminary observations made on such PACVD coatings of SiC on Pitch-55 fibres indicated that in the as-deposited form, the coatings entrap a large concentration of hydrogen, which leaves the coatings under substantial residual compressive stress. When such coated fibres are incorporated into actual metal matrix composites, molten Al must be infiltrated among them at or around 660° C. This releases the entrapped hydrogen and results in poor adhesion of fibres to matrix and in unwanted porosity. To prevent this, coatings are given outgassing treatments at 600° C to remove the hydrogen. If this process is carried to completion in a period of about 30 min at 600° C, the coatings acquire a substantial level of residual tensile stress. Thus, the type and magnitude of the residual stress in coatings is an important element in the proper performance of composites and the factors which influence it are of direct interest.

2.3. Measurement of residual stresses in coatings

The levels of residual stress in SiC coatings applied by the PACVD process were measured through the change of curvature they produce in a 25.4 mm diameter standard Si single crystal wafer with (1 0 0) surfaces and 250 μm thickness when the coating is deposited on the wafer. An initially flat and homogeneous circular disc-shaped Si wafer acquires a convex shape with a coating in residual compression on its top surface, as depicted in Fig. 1b and a concave shape when the coating is in residual tension, as depicted in Fig. 1a. Elementary considerations give readily that the residual

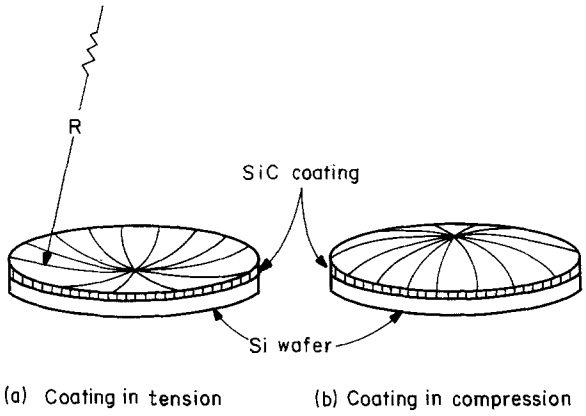

Figure 1 Change of curvature in a circular Si wafer with a thin coating of SiC in bi-axial tension (a), or in bi-axial compression (b).

bi-axial stress σ in the coating depends on the average in-plane elastic modulus E_s and the Poisson's ratio ν_s of the substrate, the thickness of h of the substrate, the thickness t of the coating and, of course, the radius of curvature R of the substrate. Provided that the coating is very much thinner than the substrate, i.e. $t/h \ll 1$, this residual stress is (Appendix 1):

$$\sigma = \frac{E_s h^2}{6(1 - \nu_s)tR}. \quad (1)$$

The residual stress is tensile for a positive curvature (concave upward) and compressive for a negative curvature (convex upward) and is not influenced by the elastic properties of the coating. The thicknesses of the coatings were measured using a Dektak II profilometer by masking portions of the Si wafer with a layer of vacuum grease before the coating was applied. When the masked areas were cleaned with a series of rinses of toluene, acetone, methanol and finally ethanol, a sharp surface step emerged at the peripheries of the coated areas left on the wafer. The height of these steps was readily measured by the diamond stylus of the profilometer (under a contact pressure of 25 mg) to an accuracy of 2.5 to 10 nm. Typical coating thicknesses which were measured were between 0.1 to 1.0 μm and were quite reproducible through control of the deposition conditions. The curvatures of the circular disc-shaped wafers with the variously stressed coatings were also measured with the same profilometer. The deformation of the bowed discs during the

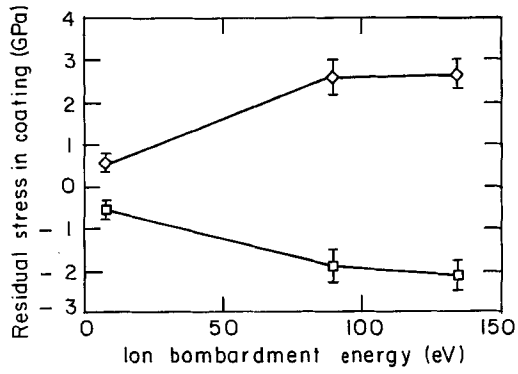

Figure 2 Measured residual stress in a PACVD SiC coating as a function of ion beam energy in both as-deposited hydrogenated coatings (compression) and coatings annealed at 600° C for 30 min. (tension). (□) as deposited; (◇) annealed.

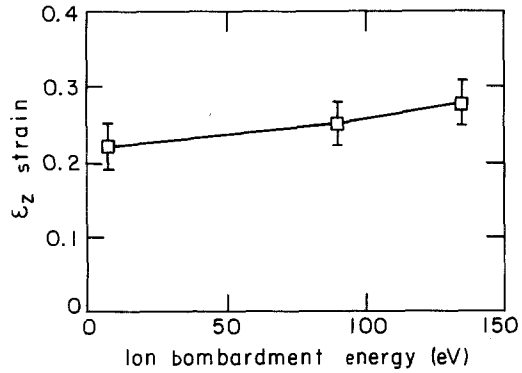

Figure 3 Thickness strain (negative) in hydrogenated coatings upon annealing at 600° C for 30 min.

measurements under the slight pressure of the stylus was negligible.

Since the maximum difference in the Young's modulus in the plane of the (1 0 0) wafer is only 16%, no important differences in curvature were detected in any orientation by the profilometer for coatings of uniform thickness. As shown in Fig. 2, the measured level of bi-axial compression in as-deposited films was found to be independent of the thickness of the deposit, but increased with increasing ion beam energy in the PACVD apparatus. Upon annealing of the as-deposited films for a period of 30 min at 600° C, copious hydrogen gas evolution from the films was observed, which resulted in substantial reduction of film thickness. This thickness reduction also increased with increasing ion beam energy, as shown in Fig. 3, indicating that more energetic ion beams result in more built-in material misfit in the films. Residual stress measurements on the wafers after the 30 min outgassing treatment at 600° C indicated that in spite of the very large reduction of thickness, the coatings also contract bi-axially and acquire a large bi-axial residual tensile stress. As Fig. 2 shows, the measured bi-axial tensile stresses in the outgassed coatings increase with initial ion beam energy in a manner symmetrical to the compressive stress in the as-deposited coatings. Clearly, these residual stresses at around 2 GPa are exceedingly high (around 0.5% of the Young's modulus of the SiC coating).

2.4. Delamination of coatings from substrates

It was observed that coatings, whether under a compressive residual stress or a tensile residual stress, delaminated nearly spontaneously from the substrate when their thickness exceeded a well-defined critical value. In both cases, delamination was initiated from interface flaws which appeared to be of circular shape and were most probably a result of occasional local surface contamination. The form of delamination in compression differed significantly from that in tension. In the former case for coatings of thickness substantially $< 1\ \mu m$, the initially circular delamination patches did not grow. However, when the coating thickness > 1 micron, slow delamination in quasi-static conditions could be observed, which initiated with outward buckling of the coating into one or two fundamental wave lengths, as can be seen in regions A of Fig. 4. These delamination patches grew by development of increasingly complex wrinkling patterns, but rapidly developed a regular delamination front, as shown for the blister at C and for the relatively large blisters in region B of Fig. 4. The blister then grew, often in neutral equilibrium, as residually stressed

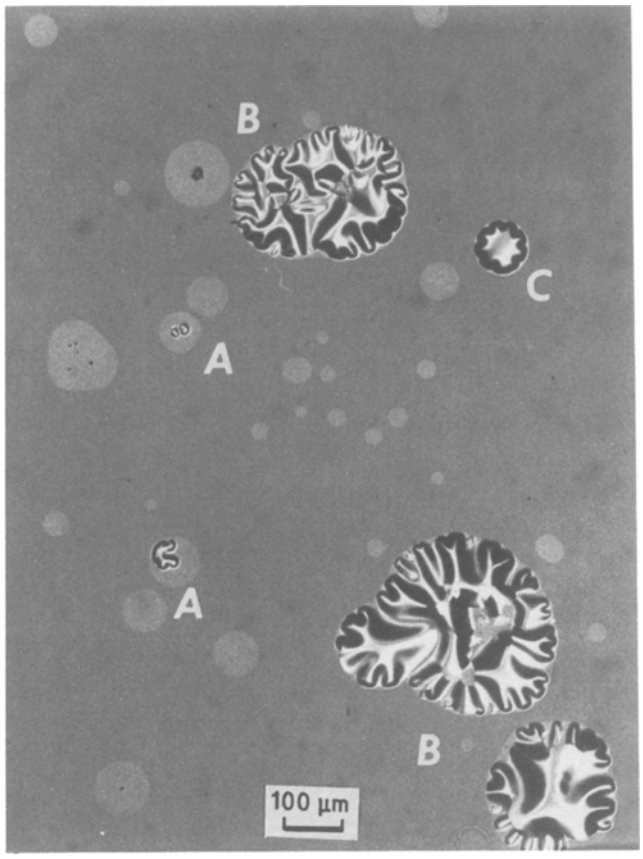

Figure 4 Blisters in the as-deposited coatings of SiC when the coatings are of a critical thickness: (A) blisters just large enough to buckle upwards, (B) large and growing blisters with well-established buckling fronts remaining self similar in growth, (C) smallest regular blister.

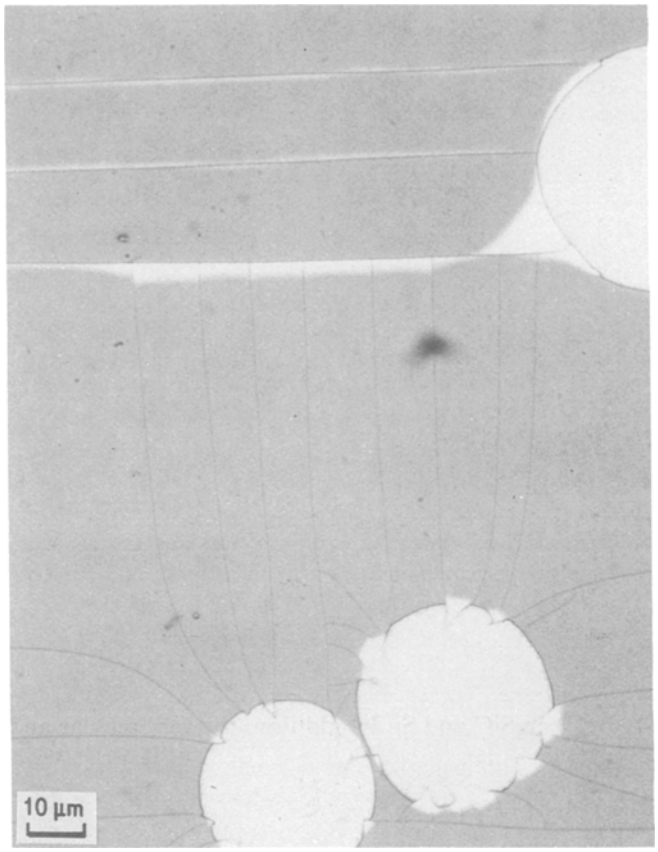

Figure 5 Detached blisters act as nucleation sites of through-the-thickness cracks in the coatings under tensile bi-axial stress, but are of insufficient thickness for delamination.

layers fed across the blister periphery into a circumferential strip with regularly spaced radial buckling ridges. In the further radial expansion of the delamination front, the principal buckling wave length in the circumferential strip immediately adjacent to the blister front remained unaltered, as can be discerned from Fig. 4 by comparing the smallest buckled blisters at A with the largest ones at B, as well as with the other intermediate sized blisters shown in the figure. Fig. 4 shows other circular patches, larger than those at A, in which no buckling has occurred. These are likely to be interface flaws, in which the adhesion of the coating to the substrate across the interface has not been fully impaired. No progressive delamination in such regions was observed.

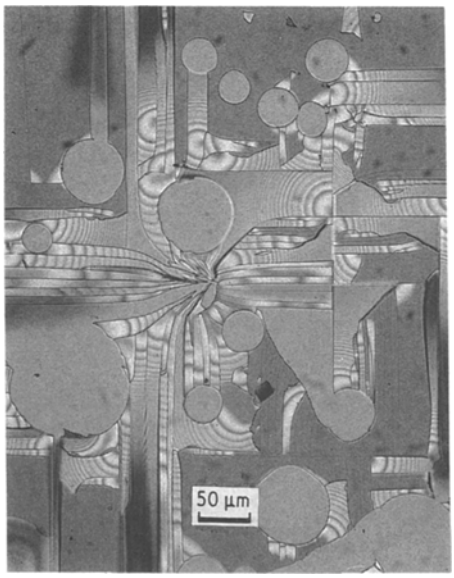

Figure 6 Delamination of ribbons from substrate, following the through-the-thickness pre-cracking of coatings under bi-axial tension when the coating is thick enough for delamination to begin.

In the outgassed samples, where the residual stress in the coating becomes bi-axial tension, the delamination shows quite different features with increasing thickness of the coating. Three different regimes of delamination have been identified in the coatings deposited under intermediate and high ion beam energies (75 to 150 eV), i.e., those in which the measured residual tensile stress was above 2 GPa. In relatively thin deposits ($< 0.2\,\mu$m thick) only circular blisters were found by the entrapment of hydrogen gas evolving during the outgassing process. In some instances, particularly for blisters of large radius, the caps of the blisters were found detached from the sample. In samples where the thickness of the coating $> 0.2\,\mu$m, blister detachment was followed by formation of cracks in the coatings emanating from the edge of the detached blister hole, as shown in Fig. 5. The initially radial cracks become parallel to one of two perpendicular directions once they are about one diameter away from the hole. The straight cracks away from the holes were found to be parallel to the two $\langle 1\,1\,0 \rangle$ directions in the plane of the Si wafer. These directions are the stiffest in the plane of the (1 0 0) wafer, and produce the largest misfit stress, across them in the coating.

In coatings that were thicker than $0.3\,\mu$m, delamination fronts spread out along the interface between the coating and the substrate bounded by the parallel pre-cracks in the coatings radiating away from the holes in the mutually orthogonal $\langle 1\,1\,0 \rangle$ directions, as shown in Fig. 6. In samples with even thicker coatings, the

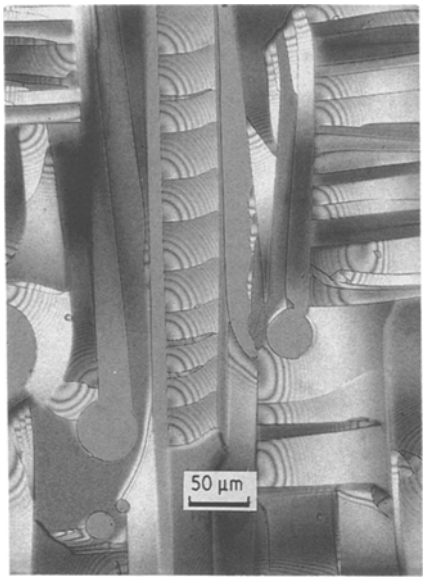

Figure 7 Regular delamination patterns in the form of long ribbons in a coating of more than sufficient thickness for delamination to occur relatively rapidly.

delaminated fraction of the interface steadily increases, as in the case of Fig. 7, until at thicknesses $> 0.75\,\mu m$, almost the entire coating has delaminated from the substrate, as is shown in Fig. 8.

Clearly, the driving force for the delamination in both cases of compressive and tensile residual stresses is the elastic strain energy in the coating. As discussed in section 2.3, the residual stress in the coating depends only on the ion beam energy and the concentration of entrapped hydrogen gas in the coating, that results in the bi-axial material misfit, but not on the coating thickness. Furthermore, as is well known and as we will demonstrate, when the coating is very much thinner than the substrate, nearly all the elastic strain energy of misfit between coating and substrate is stored in the coating. Thus, as the coating thickness increases the driving force for delamination increases nearly linearly with thickness. In very thin coatings, the stored elastic strain energy is insufficient to provide the required elastic energy release rate necessary to form the interface delamination and no delamination was found to occur in either vacuum or in air. In an intermediate range of thickness, coatings could be preserved intact when stored in a vacuum, but delaminated in time when exposed to the laboratory environment.

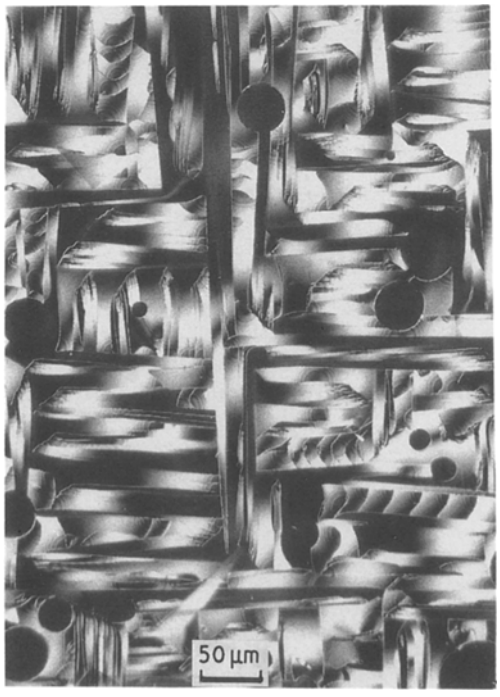

Figure 8 Nearly complete and spontaneous delamination in a coating of $0.8\,\mu m$ thickness.

With even thicker coatings, delamination occurred very rapidly both in vacuum and in air. Thus, it is expected that the delamination process along the interface is aided by humidity and is subject to static fatigue, well known in silica glasses [9]. This effect, however, will not be pursued further in this communication. We will demonstrate in section 2.6 that the observed delamination phenomenon described previously permits the rather accurate determination of the intrinsic interface toughness between a sharply delineated coating and its substrate, as is the case here between SiC and Si. In addition, the very regular and ribbon-like delamination in the case with tensile residual stresses also permits the determination of the Young's modulus of the amorphous SiC coatings. We discuss this below in the following section in preparation of the developments for interface toughness determination.

2.5. The Young's moduli of amorphous coatings in residual tension

In samples exhibiting the very regular ribbon-like delamination, it was observed that some of the loose ribbons remained perfectly flat upon delamination and in registry with the rectangular slots, in which they underwent the contractile strain resulting from the relief of the material misfit causing the residual stress. A particularly clear example of this is shown in Figs 9a and b. In Fig. 9a, the extent of the delamination ribbon is shown clearly by the bordering parallel cracks in the coating terminating $\sim 140\,\mu m$ below the horizontal crack that initiated the delamination. The termination of the grey region inside the ribbon at the point of termination of the parallel cracks indicates that the extent of delamination in the ribbon is well delineated. The upper portion of the same ribbon, given at a larger magnification in Fig. 9b, shows a well defined gap which represents the overall contraction of the ribbon upon delamination. Observations of this type, which could be made with equal precision at many places on the coating, permitted the accurate determination of the initial bi-axial misfit strain in the coating. The results of such measurements are shown in Fig. 10. They indicated that while the tensile misfit strain was quite large in coatings deposited at low ion beam energy, it was considerably smaller and independent of ion beam energy for energies $> 75\,eV$.

Since the residual tensile stress in the coatings resulting from this misfit strain could be measured separately through the measurement of the curvature of the Si wafer before any cracks could develop, as discussed in section 2.3 above, the Young's modulus

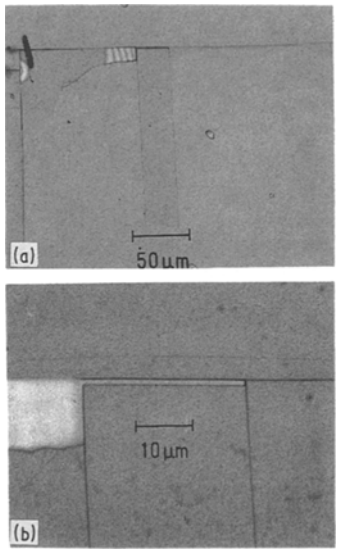

Figure 9 Misfit strain in coatings with bi-axial tensile stress is measurable by comparing the relaxed ribbon dimensions with those of the frame into which they initially fitted: (a) long delamination ribbon, (b) displacement of end of ribbon upon relief of misfit strain.

of the coatings could then be calculated from Equation (2):

$$E = \frac{(1 - \nu)\sigma}{\varepsilon_m}, \tag{2}$$

giving the dependence of bi-axial residual stress σ on the bi-axial misfit strain ε_m provided Poisson's ratio ν is known. For an assumed Poisson's ratio of 0.3, the calculated Young's moduli of SiC coatings are plotted in Fig. 11 as a function of the initial ion beam energy. The modulus goes from a rather low value of ca. 16 GPa to ~300 GPa for coatings deposited at energies > 75 eV. The determination of the Young's modulus of coatings having compressive misfit strain require a different procedure.

2.6. Work of separation of interfaces between substrates and coatings with tensile misfit

Although the stress intensity for delamination propagating along interfaces between a coating under tensile residual stress and a massive substrate of different elastic properties is complex and difficult to determine [10, 11], the associated and far more useful critical elastic energy release rate G_{co}, which we have referred to as the intrinsic interface toughness can be readily determined if the crack is constrained to remain in the interface. Thus, considering the elastic energy release from the coating and the substrate in response to a quasi-static extension of the interface crack, the desired energy release rate available from the system can be calculated readily by elementary methods from the theory of circular plates in bending (see Appendix 1) to be:

$$G_{co} \frac{\varepsilon_m^2 Et}{(1 - \nu)}\left[1 - 4\left(\frac{1 - \nu_s}{1 - \nu}\right)\left(\frac{E}{E_s}\right)\left(\frac{t}{h}\right)\right] \tag{3}$$

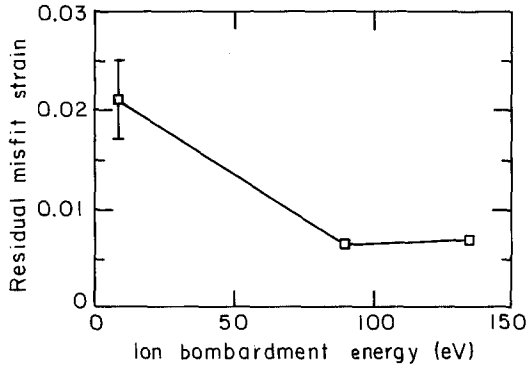

Figure 10 Dependence of bi-axial misfit strain on ion beam energy in annealed coatings under bi-axial tension.

where the second term in brackets gives the fraction of the energy released from the substrate during delamination. In Equation (3), ε_m is the total misfit strain between coating and substrate E, ν, E_s, ν_s are the Young's moduli and Poisson's ratios of the coating and substrate, respectively, and t and h are the thicknesses of the coating and substrate. For the cases of interest here $t \ll h$, and the total misfit strain is nearly entirely accommodated in the coating. Since σ and E are separately measurable, the energy release rate is calculable uniquely, provided Poisson's ratio of the coating is known. Thus, as the thickness of the coating increases, the available energy from the system becomes larger. At a given threshold thickness t_c of the coating, when the available strain energy is sufficient to provide for the total specific work of delamination in air, such delamination will occur and establishes the intrinsic interface toughness G_{co} in air as:

$$G_{co} = \frac{\sigma^2(1 - \nu)t_c}{E} \tag{4}$$

Since the work of delamination in a vacuum will be substantially larger because of the absence of static fatigue, the critical delamination thickness in vacuum for comparable conditions should be proportionally larger. The observed critical thicknesses for delamination in air are shown in Fig. 12, while the calculated specific work of delamination is shown in Fig. 13. Both of these terms depend somewhat on the ion beam energy. The average value of this work of fracture for high ion beam energies is 5.1 J m^2.

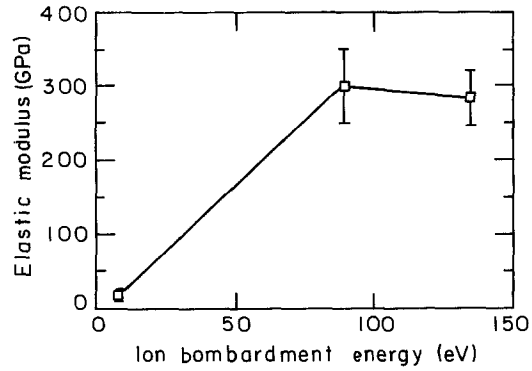

Figure 11 Dependence of Young's modulus on ion beam energy in annealed coatings under bi-axial tension.

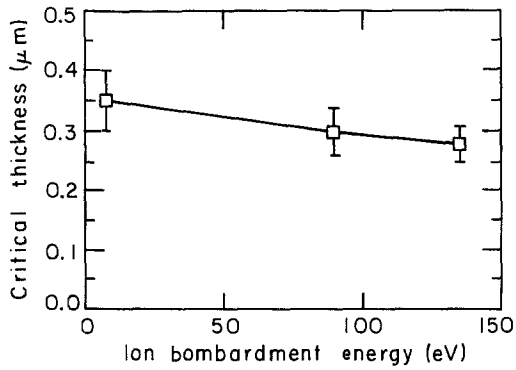

Figure 12 Dependence of critical coating thickness for delamination on ion beam energy in annealed coatings under bi-axial tension.

2.7. Work of separation of interfaces between substrates and coatings with compressive misfit

As is shown in Fig. 4 and Fig. 14a, once a sufficiently large portion of the coating is delaminated from the substrate at an initial flaw, it will undergo some release of elastic strain energy by buckling. After undergoing some early and complex buckling shapes, the delamination process settles down into a self-similar front, seen established for the blister at C in Fig. 4. In this delamination front, (Fig. 14a), bi-axially strained coating feeds in across the circumferential delamination front of the blister and undergoes nearly complete release of the radial stress. In Fig. 15, a blister is seen in Nomarski interference contrast microscopy. It reveals that the blister has an outer ring, which surrounds the buckling front at a radial distance of 5 to 7 μm ahead of it. The nature of this zone between the outer radius of this circular front and the average front of the buckled zone could not be clearly established. Since it could be seen, albeit more faintly, also in ordinary reflected light microscopy, it is attributed to an interference effect between the surface of the semi-transparent coating and the surface of the substrate. This is possible only in the presence of some cohesion impairment. We interpret it as such and propose that it results from relative radial slippage between coating and substrate. This should result then in a differential radial strain $\Delta\varepsilon_r$ and a differential thickness strain $\Delta\varepsilon_r$ given by:

$$\Delta\varepsilon_r = (1 + \nu)\varepsilon_m \qquad (5)$$

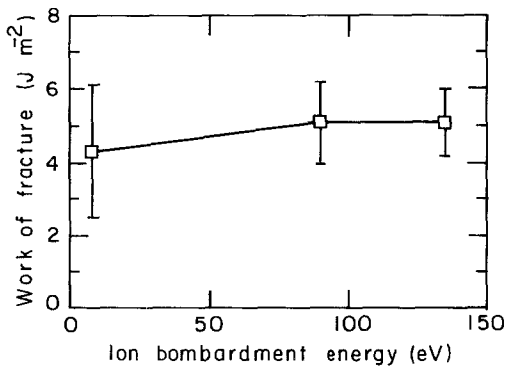

Figure 13 Dependence of critical energy release rate on ion beam energy in annealed coatings under bi-axial tension.

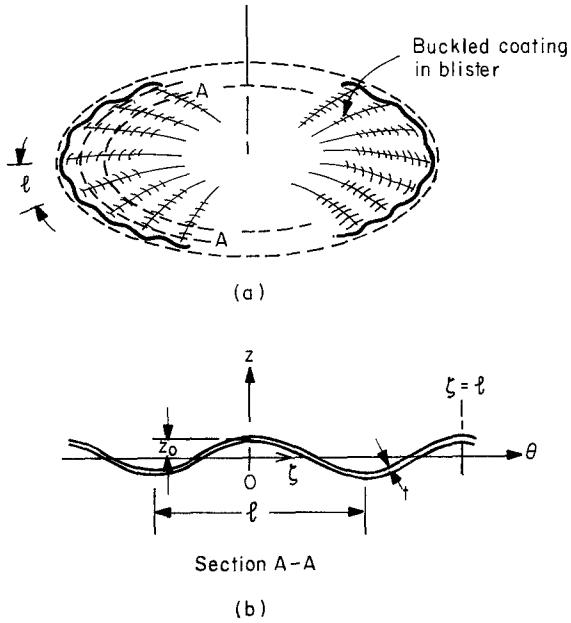

Figure 14 Sketch of idealized circumferential buckling of a delaminating coating in a blister in an as-deposited hydrogenated coating under bi-axial compression: (a) perspective view, (b) buckled coating viewed in the radial direction.

$$\Delta\varepsilon_z = -\frac{\nu(1 + \nu)}{(1 - \nu)}\varepsilon_m \qquad (6)$$

Thus, upon a critical radial displacement of the coating toward the interior of the outer front of the blister, cohesion across the interface is completely lost and the remaining tangential stress $\sigma_\theta\,(= (1 - \nu)\sigma)$ is relieved further by the regular circumferential buckling of the film to a wavelength l. The process of delamination with a self similar circumferential buckling mode becomes self-sustaining when for a radial increment of delamination, the difference between the initial elastic strain energy in the coating and that remaining in the regular post-buckling shape is sufficient to provide for the total work of delamination of the interface in this increment.

The key element of the delamination is the principal circumferential buckling wavelength l, which is directly measurable from micrographs. It relates to the initial tangential stress σ that governs it by the Euler buckling relation of thin strips, (see Appendix 2) as:

$$l = \pi t\sqrt{\frac{E}{3(1 - \nu^2)\sigma(1 - \nu)}} \qquad (7)$$

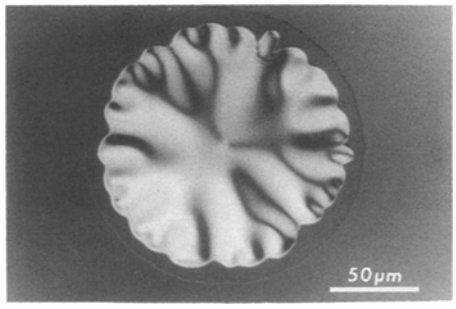

Figure 15 A large buckled blister in a coating in the process of undergoing delamination, viewed with the Nomarski interference contrast mode of microscopy. The outer ring surrounding the buckled centre is the zone in which radial slippage occurs to relieve the radial stress.

where E and ν are the Young's modulus and the Poisson's ratio of the coating as before, and σ is the initial bi-axial compressive residual stress in the coating. We note parenthetically that since the initial residual stress σ is directly measurable from the curvature of the bent wafer and l from the micrographs, the Young's modulus of the hydrogenated coating in its as-deposited form in the PACVD process is calculable directly from Equation (7).

Since the substrate is massive and nearly inextensional, once strips of coating traverse across the delamination front their initial displacement misfit in the circumferential direction must be completely relieved by the circumferential buckling. This permits calculation of the steady-state post-buckling amplitude z_0, sketched in Fig. 14b as:

$$z_0 = \frac{t}{\sqrt{3(1 - \nu^2)}} \tag{8}$$

This then permits the calculation of the final elastic strain energy U_f/unit area in the post-buckling shape of the tangential strip, just on the blister side of the delamination front to be (see Appendix 2):

$$U_f = \frac{\pi^4 E t^5}{9(1 - \nu^2)^2 l^4} \tag{9}$$

Since the initial elastic strain energy U_i/unit area in the bi-axially stressed coating in the same form of representation is:

$$U_i = \frac{\pi^4 E t^5}{9(1 - \nu^2)^2 (1 - \nu) l^4} \tag{10}$$

the elastic strain energy release rate G by this special form of tangential buckling, available to provide for the specific work of delamination of the interface becomes,

$$G = U_i - U_f = \frac{\nu \pi^4 E t^5}{9(1 - \nu^2)^2 (1 - \nu) l^4} \tag{11}$$

Once again, at a critical thickness t_c, this energy becomes sufficient to provide for the quasi-static propagation of the delamination front in neutral equilibrium in air, establishing the intrinsic delamination toughness of the interface G_{co} as:

$$G_{co} = \frac{\nu \pi^4 E t_c^5}{9(1 - \nu^2)^2 (1 - \nu) l^4} \tag{12}$$

As a specific case, we consider the delamination blisters of Fig. 4 of a coating deposited at high ion beam energy, expected to have a bi-axial compressive residual stress of $\sigma = 2$ GPa, as shown in Fig. 2. The critical thickness of this coating was measured to be 1.1 μm, while the average post-buckling wave length l in the circumferential direction was measured to be 20 μm. Assuming as before a Poisson's ratio of 0.3, we calculate first the Young's modulus from Equation (7) to be 116 GPa. Finally, using this value, the critical energy release rate G_{co} (specific work of delamination) is calculated from Equation (12) to be 5.9 J m^2. This is 14% higher than the average value calculated from the delamination of the coatings under tensile residual stress and well within the scatter of measurements of that experiment. Thus we conclude that the intrinsic toughness of the interface between SiC and Si is uninfluenced by the dehydrogenation that converts the coatings from having negative misfit to positive misfit.

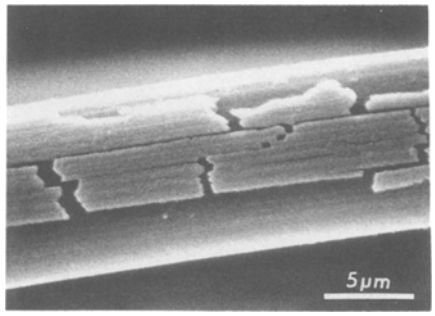

Figure 16 An SEM micrograph of a fragmented and delaminated annealed coating of critical thickness of SiC on a Pitch-55 fibre. The misfit strain is determinable from the gaps between the flakes.

3. Toughness of interfaces between SiC coatings and Pitch-55 fibres

The total work of delaminating a SiC coating from a Pitch-55 carbon fibre can also be determined by a technique very similar to that used for a system of Si wafer and SiC coating under tensile misfit strain. Fig. 16 shows a SEM micrograph of an outgassed fibre with a SiC coating of 0.33 μm thickness, initially deposited under conditions of low ion beam energy. The coating showed some small through the thickness cracks, but no delamination during several weeks of storage in air after the regular outgassing treatment of 30 min at 600° C. When it was examined again after several months of further storage in laboratory air with the usual level of relative humidity, in the vicinities of 60%, copious delamination of the SiC coating was found, as shown in Fig. 16. The initial bi-axial misfit strain ε_m between the coating and the fibre could be determined from the ratio of the average gap size between flakes to the dimensions of the flakes. With knowledge of this, and the assumption that the Young's modulus of the coating was the same as that for similar coatings on Si wafers deposited under the same ion beam conditions, the total energy release rate per unit area of interface could be determined from the sample.

An elementary misfit analysis presented in more detail in Appendix 3 gives the intrinsic interface toughness G_{co} of the interface to be

$$G_{co} = \frac{\varepsilon_m^2 E t_c}{2} \left(\frac{F}{H^2} \right) \tag{15}$$

where ε_m is the bi-axial misfit strain between coating and fibre, E the Young's modulus of the coating, t_c the thickness of the coating, and F and H are complicated functions of ratios of Young's moduli and the coating thickness to fibre radius given as:

$$F = 2(1 - \nu) + \left[(3 - 5\nu) \left(\frac{E}{E_r} \right) + 6(1 - \nu) \left(\frac{E}{E_z} \right) \right] \left(\frac{t}{R} \right)$$

$$+\left[(1-2\nu)\left(\frac{E}{E_r}\right)^2+4(1-\nu)\left(\frac{E}{E_z}\right)^2\right.$$
$$\left.+2(4-7\nu)\left(\frac{E}{E_r}\right)\left(\frac{E}{E_z}\right)\right]\left(\frac{t}{R}\right)^2$$
$$+2\left[(1-2\nu)\left(\frac{E}{E_r}\right)\left(\frac{E}{E_z}\right)\left(\frac{E}{E_r}+\frac{2E}{E_z}\right)\right]\left(\frac{t}{R}\right)^3 \quad (14)$$

$$H = (1-\nu)+\left[(1-2\nu)\left(\frac{E}{E_r}\right)\right.$$
$$\left.+2(1-\nu)\left(\frac{E}{E_z}\right)\right]\left(\frac{t}{R}\right)$$
$$+2(1-2\nu)\left(\frac{E}{E_r}\right)\left(\frac{E}{E_z}\right)\left(\frac{t}{R}\right)^2 \quad (15)$$

In Equations (14) and (15), (E/E_r) and (E/E_z) are the ratios of the Young's modulus of the coating to the transverse modulus of the fibre and the axial modulus of the fibre respectively; ν is the Poisson's ratio of both the fibre and the coating (assumed to be the same) and t/R is the ratio of the thickness of the coating to the fibre radius.

As a specific example, we evaluate the critical energy release rate of the coating related to the case of Fig. 16 of a coating applied to a fibre under low ion beam conditions in the PACVD apparatus. This should result in a coating with Young's modulus of $E = 16\,\text{GPa}$. The initial misfit strain, as measured from the gaps between the fragments of the coatings was found to be $\varepsilon_m = 2.7 \times 10^{-2}$ in the axial direction. Since the axial and radial Young's moduli E_z and E_r of the fibre were 385 GPa and 14 GPa respectively, $E/E_r = 1.14$ and $E/E_z = 4.16 \times 10^{-2}$. Furthermore, thickness of the SiC coating was 0.33 μm and the fibre radius 5 μm, giving $t/R = 6.6 \times 10^{-2}$. Thus, for assumed Poisson's ratios of 0.3, the values of the functions F and H can be calculated to be 1.53 and 0.734 respectively. This gives for the intrinsic interface toughness $G_{co} = 5.5\,\text{J m}^2$, which is very close to the corresponding value measured for the delamination of the interface between SiC and a Si substrate.

4. Discussion

We have demonstrated that the spontaneous delamination phenomenon of thin misfitting coatings from their substrates can be used very effectively to determine the toughness of the interface between them. When the elastic strain energy per unit area due to the misfit in the coating begins to exceed the intrinsic interface toughness, i.e., the specific work of separation of the coating from the substrate along the interface, the coating delaminates from the interface flaws. Since no instability is involved, the delamination, once started, can propagate under quasi-static conditions. Observations indicate that the critical thickness of a coating for delamination in vacuum is larger than the corresponding thickness for delamination in laboratory air with the usual levels of relative humidity. Thus, a static fatigue or stress corrosion cracking effect appears to be present in the delamination. This aspect of the delamination still needs to be studied further.

When the coatings are in residual tension, the delamination occurs in a sequence of events, beginning with cracking of the coating in long parallel rows, followed by delamination of the ribbons of coating between the parallel cracks. Since the substrate Si wafers had {1 0 0} plane surfaces in which the two orthogonal ⟨1 1 0⟩ directions are 16% stiffer than the ⟨1 0 0⟩ directions, the resulting larger misfit stresses in the ⟨1 1 0⟩ directions produce these orthogonal pre-cracks in the coatings. The misfit strain could be measured quite accurately from the relaxed size of the delaminated loose ribbon lying flat in the rectangular cavity of pre-cracking. This, together with the independent measurement of the residual tensile stress through the curvature of the sandwich of coating and substrate, permitted the determination of the elastic modulus of the coatings, which is essential for the determination of the energy release rate.

When the coatings are in residual compression in the hydrogenated state, immediately upon coating, the delamination exhibited rather unusual and hitherto unreported forms. When the coating exceeded the critical thickness required to provide the energy release rate, delamination occurred by the enlargement of blisters having self similar circumferential fronts, in which first, the radial stress appears to be released by translation of the coating relative to the substrate in the radial direction by an amount

$$\Delta u_r = \Delta r \Delta \varepsilon_r \quad (16)$$

where Δr is the width of the radial stress release zone of about 5 μm thickness, shown in Fig. 15, and $\Delta\varepsilon_r$ is the radial strain difference between coating and substrate in this zone, given by Equation (5). For the typical case considered in section 2.7 above, where for a residual compressive stress of 2 GPa and a coating modulus of 116 GPa, giving an initial misfit strain of 1.21×10^{-2}, the relative displacement in the inner border of the radial stress release zone is obtained to be ca. 60 nm. The degree of reduction of shear traction in this radial zone is unknown. We consider it to be substantially reduced, but the coating is still attached to the substrate even after a relative slippage of hundreds of interatomic distances. If this interpretation is indeed correct, it must be concluded that for flat interfaces, there is little reduction of the cohesive strength of an interface due to large relative shear displacements across it. Although this is quite natural for flat grain boundaries, it is surprising for the interfaces between crystalline Si and amorphous SiC. Finally, however, as the relative displacements across this strip mount, small departures from flatness should produce normal stresses acting across the interface to produce full delamination and the quite regular circumferential buckling that is so readily apparent. It is interesting to note that the buckled blisters require only one independent measurement for the complete solution of the problem. Considering that the thickness of the coating and the wavelength of

the circumferential buckling are readily determinable by microscopy, only the residual compressive stress in the coating needs to be measured separately by measuring the radius of curvature of the sandwich of Si wafer and SiC coating. The Young's modulus of the coating can be determined from Equation (7), making the energy-release rate determinable uniquely from Equation (12).

The measurement of real interest for metal matrix composites, however, is the interface toughness between a SiC coating and a Pitch-55 carbon fibre, which could be determined by a similar analysis, provided the modulus of the coating depends only on the energy of the ion beam and not on any other property of the substrate or condition of deposition. This point needs to be verified further by additional experiments with planar surfaces of Pitch-55 type material in thin strips permitting residual stress measurement by curvature change. Meanwhile, in the absence of this information, the determined interface toughness of $5.5\,J\,m^2$ is, within experimental error, identical to that between SiC and Si. Furthermore, in the latter case, there was no effect on the interface toughness of substantial residual stresses in the plane of the coating, whether tensile or compressive. The overall average value of the interface toughness for the three experiments is $5.5\,J\,m^2$. It is interesting to compare this overall interface toughness with fundamental expectations. In the absence of any inelastic deformation the intrinsic toughness of an interface should be:

$$G_{co} = \chi_A + \chi_B - \chi_{AB} \tag{17}$$

where χ_A and χ_B can stand for the surface free energies of SiC (A), and Si or C (B), and χ_{AB} for the interface energy of one or the other pair of Si/SiC or C/SiC. Considering more specifically the pair of Si/SiC we note that $\chi_{Si} = 1.24\,J\,m^2$ [12], while no information is available for χ_{SiC} and $\chi_{Si/SiC}$. Taking χ_{SiC} as $\chi_{Si}(E_{SiC}/E_{Si})$ as a zero order approximation, we obtain for $\chi_{SiC} = 2.53\,J\,m^2$. Furthermore, guessing for $\chi_{Si/SiC}$ a value of $1.00\,J\,m^2$, we obtain for $G_{co} = 2.77\,J\,m^2$. This is only about one half of what was measured. Although it is possible that interface slippage can be responsible for the difference in energy, this does not fully account for the observations. The delamination remains on the interface and does not veer into the substrate or the coating, where the intrinsic toughness levels would appear to be lower. Thus, on the basis of the above estimates we must conclude that either our measurements still contain an error of a factor of 2 or that the effective fracture toughness of the two substrates are actually higher than twice their respective surface energies. It is likely that a combination of these two explanations is responsible for the observations.

Acknowledgements

We gratefully acknowledge DARPA, US Office of Naval Research and US Naval Air Development Center under Contract No. N00014-84-K and IST/SDIO under Contract No. N00014-85-K-0645 and the M.I.T. Consortium for Processing and Evaluation of Metal and Ceramic Matrix Composites for their generous support of this project. We are also grateful to Dr J. Cuomo of IBM for his advice on PACVD facility design, and to Professor A. Mortensen for discussions on delamination of compression blisters.

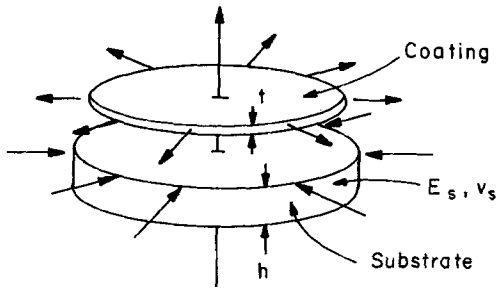

Figure 17 Misfit between coating and substrate in round disc.

Appendix 1. Residual stress measurements in thin coatings and interface toughness from coatings in tension

Consider a thin circular wafer with (1 0 0) plane surfaces, having a thickness h, an in-plane isotropic modulus of E_s, and a Poisson's ratio of ν_s. An amorphous isotropic coating of thickness t of SiC with modulus E_c and Poisson's ratio ν_c is attached to the substrate. Due to the condition of deposition, the coating incorporates a bi-axial misfit strain ε_m, which we take to be tensile. This puts it under a state of residual tensile stress $\sigma_r (= \sigma_\theta)$, which is of interest. As all elastic misfit problems, the solution is obtained by detaching the coating from the substrate, as shown in Fig. 17 and considering the deformations necessary to attach them together again. Thus, considering the coating to be so thin as to be under a uniform stress σ_r, by equilibrium, the substrate would be subjected to a compressive stress $\sigma_r(t/h)$ and a bending moment per unit length of periphery of:

$$M = (\sigma_r t)(t + h)/2 \tag{A1}$$

This bending moment produces a spherical curvature in the substrate wafer given by:

$$\frac{1}{R} = \frac{M}{D_s(1 + \nu_s)} \therefore D_s = \frac{E_s h^3}{12(1 - \nu_s)^2} \tag{A2}$$

and a surface strain at the interface of:

$$\varepsilon_r = \frac{h}{2R} \tag{A3}$$

The average compressive stress in the wafer produces an average radial compressive strain of:

$$\varepsilon_r = \frac{(1 - \nu_s)\sigma_r t}{hE_s} \tag{A4}$$

The sum of all radial strains at the interface in the coating and the substrate must be equal to the initial misfit strain ε_m:

$$\varepsilon_m = \frac{(1 - \nu_c)\sigma_r}{E_c} + \frac{(1 - \nu_s)\sigma_r t}{hE_s} + \frac{t(t + h)h\sigma_r}{4D_s(1 + \nu_s)} \tag{A5}$$

where the first term is the radial strain in the coating.

Thus:

$$\varepsilon_m = \left[\frac{(1-\nu_c)}{E_c} + \frac{4(1-\nu_s)}{E_s}\left(\frac{t}{h}\right) + \frac{3(1-\nu_s)}{E_s}\left(\frac{t}{h}\right)^2\right]\sigma_r \quad \text{(A6)}$$

On the other hand, from Equation (A2), the bi-axial stress σ in the coating is:

$$\sigma = \sigma_r = \frac{E_s h^3}{6t(1-\nu_s)(t+h)R} \approx \frac{E_s h^2}{6t(1-\nu_s)R}\left(1 - \frac{t}{h}\right) \quad \text{(A7)}$$

Thus, through the measurement of the radius of curvature of the bent wafer, the residual stress in the coating is determinable from Equations (A7).

The elastic strain energy stored in the sandwich of stretched coating, and compressed and bent substrate is determinable in a straightforward way from the theory of thin circular plates. The strain energy in the coating is determinable from Equation (A7).

$$\frac{(1-\nu_c)\sigma^2 t}{E_c} \quad \text{(A8)}$$

In the substrate, the elastic strain energy is partly in bending, of a magnitude of:

$$\frac{3(1-\nu_s)t^2}{E_s h}\left(1 + 2\left(\frac{t}{h}\right)\right)\sigma^2 \quad \text{(A9)}$$

and partly in compression, of a magnitude of:

$$\frac{(1-\nu_s)h}{E_s}\sigma^2\left(\frac{t}{h}\right)^2 \quad \text{(A10)}$$

Thus, the total elastic strain energy, U is the sandwich is the sum of all three terms, which for quantities including second order terms is:

$$U = \frac{\varepsilon_m^2 E_c t}{(1-\nu_c)}\left[1 - 4\frac{(1-\nu_s)}{(1-\nu_c)}\frac{E_c}{E_s}\left(\frac{t}{h}\right)\right] \quad \text{(A11)}$$

where the total misfit strain is:

$$\varepsilon_m = \frac{\sigma(1-\nu_c)}{E_c}\left[1 + 4\frac{(1-\nu_s)}{(1-\nu_c)}\frac{E_c}{E_s}\left(\frac{t}{h}\right)\right] \quad \text{(A12)}$$

In Equation (A11), the second term in the brackets is the fraction of the energy contributed to the total through the bending and compression of the substrate. For $t/h \ll 1$, this contribution is clearly negligible. This gives for the elastic energy release rate in delamination

$$G_{co} = U \simeq \frac{\varepsilon_m^2 E_c t}{(1-\nu_c)} \quad \text{(A13)}$$

which was used in the interpretation of results.

Appendix 2 Interface toughness from buckled blisters

As explained in the text, the coating inside a blister lifts off through the propagation of a circumferential buckling front with a characteristic circumferential wavelength of l.

Initially, under bi-axial compression, the stresses in the coating are:

$$\sigma_r = \sigma_\theta = \frac{E\varepsilon_r}{(1-\nu)} = \frac{E\varepsilon_\theta}{(1-\nu)} = \frac{E\varepsilon_m}{(1-\nu)} \quad \text{(A14)}$$

where E and ν are properties of the coating, and ε_m the total misfit strain.

Upon traverse of the outer fringe of the blister through an element of coating, the radial stress is fully released; this reduces the tangential stress down to:

$$\sigma_\theta = E\varepsilon_\theta. \quad \text{(A15)}$$

As the element of coating traverses through the buckling front, it undergoes a characteristic Euler buckling that responds to the new level of tangential stress, and establishes a circumferential buckling wavelength of

$$l = \pi t\sqrt{\frac{E}{3(1-\nu^2)\sigma_\theta}} \quad \text{(A16)}$$

In the post-buckling shape, circumferential line elements in the coating become longer by an amount of $l\varepsilon_m$ over a wavelength of buckled coating

$$\Delta l = l\varepsilon_m = \frac{\pi^2 t^2}{3l(1-\nu^2)} \quad \text{(A17)}$$

This establishes the amplitude of buckling along a circumferential line element. Thus, in reference to Fig. 14b:

$$\Delta l = \int_0^l \left(\sqrt{1 + \left(\frac{dz}{d\phi}\right)^2} - 1\right)d\phi = \frac{\pi^2 z_0^2}{l} \quad \text{(A18)}$$

for a sinusoidal buckling shape:

$$z = z_0 \sin\left(\frac{2\pi\phi}{l}\right), \quad \text{(A19)}$$

giving for the amplitude:

$$z_0 = \frac{t}{\sqrt{3(1-\nu^2)}} \quad \text{(A20)}$$

The final elastic strain energy in the post-buckling shape per unit width in the radial direction is:

$$U_f = \int_0^l \frac{M^2}{2EI}d\phi \;\therefore\; M = EI\frac{d^2 z}{d\phi^2} \quad \text{(A21)}$$

giving

$$U_f = \frac{4EI\pi^4 z_0^2}{l^3} = \frac{\pi^4 E t^5}{9l^3(1-\nu^2)^2} \quad \text{(A22)}$$

The initial elastic strain energy in the bi-axially strained coating per strip of unit width and length l is:

$$U_i = \frac{(1-\nu)\sigma_\theta^2 lt}{E} = \frac{\pi^2 E t^5}{9(1-\nu^2)^2(1-\nu)l^3} \quad \text{(A23)}$$

where

$$\sigma_\theta = \frac{\pi^2 E t^2}{3(1-\nu^2)(1-\nu)l^2} \quad \text{(A24)}$$

the initial tangential stress was substituted to obtain the final result. Finally, the energy release rate (per

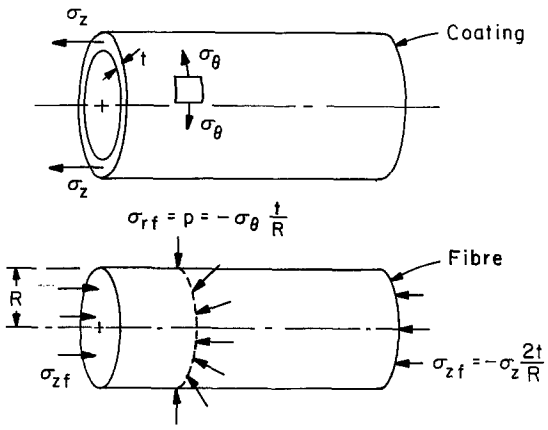

Figure 18 Misfit between coating and fibre.

unit area of coating) is obtained by subtraction of (A9) from (A10), and dividing by l:

$$G_{co} = \frac{v\pi^4 Et^5}{9(1 - v^2)^2(1 - v)l^4} \quad \text{(A25)}$$

Appendix 3 Interface toughness of coatings on Pitch-55 fibres

Consider a Pitch-55 type fibre of radius R with an axial modulus E_z, a radial modulus E_r, and Poisson's ratio v with an isotropic coating of thickness t, with a modulus E and Poisson's ratio v, having a total tensile bi-axial misfit strain ε_m relative to the fibre. As indicated in Fig. 18, we take the unknown misfit stresses in the coating to be σ_θ and σ_z, and since $t/R \ll 1$ will be the case, neglect radial stresses. The corresponding stresses in the fibre that result from equilibrium are given in the figure.

By straightforward analysis, the strains in the coating and the fibre are:

$$\varepsilon_{\theta c} = \sigma_\theta/E - v\sigma_z/E \therefore \varepsilon_{zc} = \sigma_z/E - v\sigma_\theta/E \quad \text{(A26)}$$

$$\varepsilon_{\theta f} = -(1 - v)t\sigma_\theta/E_r R + 2vt\sigma_z/E_z R \quad \text{(A27)}$$

$$\varepsilon_{zf} = 2vt\sigma_\theta/E_r R - 2t\sigma_z/E_z R \quad \text{(A28)}$$

The matching of the fibre to the coating requires:

$$\varepsilon_{\theta c} - \varepsilon_{\theta f} = \varepsilon_m \therefore \varepsilon_{zc} - \varepsilon_{zf} = \varepsilon_m \quad \text{(A29)}$$

This gives by elementary methods:

$$\sigma_\theta = \frac{\varepsilon_m E}{H}\left[1 + 2\left(\frac{E}{E_z}\right)\left(\frac{t}{R}\right)\right] \quad \text{(A30)}$$

$$\sigma_z = \frac{\varepsilon_m E}{H}\left[1 + \frac{E}{E_r}\left(\frac{t}{R}\right)\right] \quad \text{(A31)}$$

where

$$H = (1 - v) + \left[(1 - 2v)\frac{E}{E_r} + 2(1 - v)\frac{E}{E_z}\right]\left(\frac{t}{R}\right) + 2(1 - 2v)\left(\frac{E}{E_r}\right)\left(\frac{E}{E_z}\right)\left(\frac{t}{R}\right)^2 \quad \text{(A32)}$$

The elastic strain energy in the fibre and coating per unit length are:

$$U_f = (\sigma_{\theta f}\varepsilon_{\theta f} + \sigma_{zf}\varepsilon_{zf}/2)\pi R^2 \quad \text{(A33)}$$

$$U_c = (\sigma_\theta^2 + \sigma_z^2 - 2v\sigma_\theta\sigma_z)\pi Rt/E \quad \text{(A34)}$$

By elementary methods, using the results above, the total elastic strain energy/unit length of fibre can be readily obtained as:

$$U = \frac{\pi Rt\varepsilon_m^2 E}{H^2} F \quad \text{(A35)}$$

where

$$F = 2(1 - v) + \left[(3 - 5v)\left(\frac{E}{E_r}\right) + 6(1 - v)\left(\frac{E}{E_z}\right)\right]\left(\frac{t}{R}\right) + \left[(1 - 2v)\left(\frac{E}{E_r}\right)^2 + 4(1 - v)\left(\frac{E}{E_z}\right)^2 + 2(4 - 7v)\left(\frac{E}{E_r}\right)\left(\frac{E}{E_z}\right)\right]\left(\frac{t}{R}\right)^2 + 2(1 - 2v)\left(\frac{E}{E_r}\right)\left(\frac{E}{E_z}\right)\left(\frac{E}{E_r} + 2\left(\frac{E}{E_z}\right)\right)\left(\frac{t}{R}\right)^3 \quad \text{(A36)}$$

This gives finally the energy release rate per unit area of interface, if delamination were to occur at the interface to completely unload both fibre and coating:

$$G_{co} = U/2\pi R = \frac{\varepsilon_m^2 EtF}{2H^2}. \quad \text{(A37)}$$

This was used to evaluate the results of cracking and delamination of coatings from fibres.

References

1. K.L. MITTAL, in "Adhesion Measurement of Thin Films, Thick Films, and Bulk Coatings", edited by K. L. Mittal, ASTM STP 640 (American Society for Testing and Materials, Philadelphia, 1978) p. 5.
2. T. S. CHOW, C. A. LIU and R. C. PENWELL, *J. Polymer Sci.* **14** (1976) 1305.
3. J. AHN, K. L. MITTAL and R. H. McQUEEN, in "Adhesion Measurement of Thin Films, Thick Films, and Bulk Coatings", edited by K. L. Mittal, ASTM STP 640 (American Society for Testing and Materials, Philadelphia, 1978) p. 134.
4. S. S. CHIANG, D. B. MARSHALL and A. G. EVANS, in "Surfaces and Interfaces in Ceramic and Ceramic Metal Systems", edited by J. Pask and A. G. Evans (Plenum Press, New York, 1981) Vol. 14, p. 603.
5. J. R. RICE, in Proceedings of First International Conference on Fracture, Sendai, Japan, Vol. 1, edited by T. Yokobori, T. Kawasaki and J. L. Swedlow (The Japanese Society for Strength and Fracture of Materials, Sendai, Japan, 1965) p. 309.
6. V. GUPTA, A. S. ARGON and J. A. CORNIE, *J. Mater. Sci.* to be published.
7. A. G. EVANS and J. W. HUTCHINSON, *Intern. J. Solids and Structures* **20** (1984) 455.
8. H. S. LANDIS, Amorphous Hydrogenated Silicon Carbide by Plasma Enhanced Chemical Vapor Deposition for Metal Matrix Composite Applications, PhD thesis, Department of Materials Science and Engineering, M.I.T., Cambridge, Massachusetts, USA (1987).
9. S. W. FREIMAN, in "Glass Science and Technology", edited by D. R. Uhlmann and N. J. Kreidl (Academic Press, New York, 1980) Vol. 2, p. 21.
10. J. R. RICE and G. S. SIH, *J. Appl. Mech.* **32** (1965) 418.
11. M. COMNINOU, *ibid.* **44** (1977) 631.
12. J. J. GILMAN, *J. Appl. Phys.* **31** (1960) 2208.

Received 13 March
and accepted 8 July 1988